APS physics

CHORUS

This is the accepted manuscript made available via CHORUS. The article has been published as:

Self-consistent theory of nanodomain formation on nonpolar surfaces of ferroelectrics

Anna N. Morozovska, Anton V. Ievlev, Vyacheslav V. Obukhovskii, Yevhen Fomichov, Oleksandr V. Varenyk, Vladimir Ya. Shur, Sergei V. Kalinin, and Eugene A. Eliseev

Phys. Rev. B **93**, 165439 — Published 28 April 2016

DOI: 10.1103/PhysRevB.93.165439

Resubmitted to Phys.Rev.B.

Self-consistent theory of nanodomain formation on non-polar surfaces of ferroelectrics

Anna N. Morozovska[1*], Anton V. Ievlev[2,3], Vyacheslav V. Obukhovskii[4], Yevhen Fomichov[5], Oleksandr V. Varenyk[1], Vladimir Ya. Shur[6], Sergei V. Kalinin[2,3] and Eugene A. Eliseev[5†]

[1] Institute of Physics, National Academy of Science of Ukraine,
46, pr. Nauky, 03028 Kyiv, Ukraine

[2] The Institute for Functional Imaging of Materials, Oak Ridge National Laboratory,
Oak Ridge, TN 37831

[3] The Center for Nanophase Materials Sciences, Oak Ridge National Laboratory,
Oak Ridge, TN 37831

[4] Taras Shevchenko Kyiv National University, Radiophysical Faculty
4g, pr. Akademika Hlushkova, 03022 Kyiv, Ukraine

[5] Institute for Problems of Materials Science, National Academy of Science of Ukraine,
3, Krjijanovskogo, 03142 Kyiv, Ukraine

[6] Institute of Natural Sciences, Ural Federal University,
51 Lenin Ave., 620000, Ekaterinburg, Russia.

Abstract

We propose a self-consistent theoretical approach capable to describe the features of the anisotropic nanodomain formation induced by a strongly inhomogeneous electric field of charged SPM tip on non-polar cuts of ferroelectrics. We obtained that a threshold field, previously regarded an isotropic parameter, is an anisotropic function that is specified from the polar properties and lattice pinning anisotropy of a given ferroelectric in a self-consistent way. The proposed method for the calculation of the anisotropic threshold field is not material-specific, thus the field should be anisotropic in all ferroelectrics with the spontaneous polarization anisotropy along the main crystallographic directions. The most evident examples are uniaxial ferroelectrics, layered ferroelectric perovskites and low symmetry incommensurate ferroelectrics. Obtained results quantitatively describe difference in several times in nanodomain length experimentally observed on X- and Y-cuts of $LiNbO_3$ and can give insight into the anisotropic dynamics of nanoscale polarization reversal in strongly inhomogeneous electric fields.

[*] Corresponding author 1: anna.n.morozovska@gmail.com

[†] Corresponding author 2: eugene.a.eliseev@gmail.com

I. Introduction

The investigation of local polarization dynamics in ferroelectric materials becomes one of the most intriguing and rapidly developed direction of fundamental studies in nano-physics as well as prospective for next generation of memory devices [1, 2, 3, 4, 5, 6, 7]. The reason that made the investigations very attractive is the possibility to control the local redistribution of ferroelectric polarization, in particular to form the nanodomains arrays by the strongly inhomogeneous electric field of scanning probe atomic force microscopy (SPM) tip [8, 9].

There are many experimental and theoretical studies of nanodomain formation on polar surfaces of ferroelectric crystals by the biased SPM probe, demonstrating that the normal [10, 11, 12, 13, 14, 15, 16, 17] or anomalous [18, 19, 20, 21] local polarization reversal can take place along a polar axis. Experimental studies of the micro- and nano- domain walls motion have been performed in typical crystalline ferroelectric materials such as Pb(Zr, Ti)O_3, $Pb_5Ge_3O_{11}$, $LiTaO_3$, $LiNbO_3$ [22, 23, 24, 25]. Appeared that the lateral sizes of micro- and nano-domain are linearly proportional to the voltage pulse amplitude and to the logarithm of the pulse duration [8, 10].

A number of semi-phenomenological models of the nanodomain formation caused by the strongly inhomogeneous electric field produced by the SPM tip have been proposed. These models can be conditionally divided into two groups, namely Landauer-Molotskii (LM) energetic approach [9, 26, 27, 28, 29, 30, 31] and Landau-Ginzburg-Devonshire (LGD) approach [32, 33, 34, 35, 36, 37]. LM approach considers the semi-ellipsoidal domain with infinitely thin walls and includes the domain wall surface energy into the free energy functional. LGD approach allows calculations of the domain shape, sizes and wall thickness in a self-consistent way, as a solution of the relaxation-type time-dependent nonlinear differential Landau-Ginzburg-Devonshire-Khalatnikov (TD-LGD or LGDK) equation for the evolution of ferroelectric polarization distribution coupled with the Poisson equation for the electric field, bound and space charges determination.

Almost all experimental and theoretical papers are devoted to the investigation of the nanodomain kinetics on polar ferroelectric surfaces; at the same time the forward growth remains one of the most unexplored stages due to lack of experimental methods allowing investigations in the bulk. Recently Ievlev et al [35] and Alikin et al [38] experimentally demonstrated that the tip-induced polarization reversal on nonpolar X- and Y- cuts in a single crystal of congruent $LiNbO_3$ can give insight in the forward growth on the nanoscale. They reported significant deviation of the domain shape from a semi-ellipsoid as well as the difference of the domain shapes and sizes on X- and Y-cuts (see **Figure 1**), which contradicts to the recent theoretical calculations by Pertsev et al [39] using thermodynamic LM approach. Alikin et al concluded that their results can be explained only in terms of kinetic approach, which self-consistent formulation is absent to date.

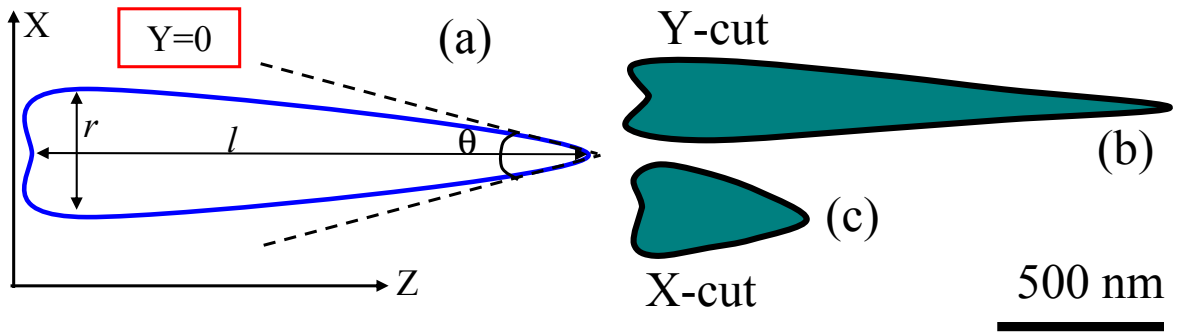

Figure 1. **(a)** Sketch of the domain shape in the XZ plane (Y=0) induced by AFM probe on congruent $LiNbO_3$ (CLN) non-polar cuts. **(b-c)** Experimentally observed domain shape from Alikin et al [38] on **(b)** Y- and **(c)** X-cuts of 20-μm-thick CLN.

It is well-established that the domain wall kinetics is strongly affected by the lattice pinning [40], which was not accounted in the classical LGD approach. Lattice pinning phenomenon is based on the fact that the domain wall can move over a distance equal to the integer number of lattice constants. In this case critical electric fields, required for the local polarization reversal, are defined by the interplay between the pinning, depolarization and tip fields and can be estimated analytically using several models. Suzuki-Ishibashi (S-I) model [41] can be used for the threshold field determination. The activation filed, that determines the nucleation kinetics, can be defined within Miller-Weinreich [42] or Burtsev-Chervonobrodov (B-C) models [43] modified by Rappe et al [44] and Aravind et al [34] respectively by inclusion the phenomena related with polarization gradient and depolarization effects at the domain wall. However, none of the models account for the possible anisotropy of the threshold and activation fields in different directions. Consequently all of them cannot describe the anisotropic domain growth revealed experimentally [38].

Aforementioned facts motivated us to develop the quantitative self-consistent description of the anisotropic nanodomain formation and growth on the non-polar ferroelectric surfaces. We propose the conception of the anisotropic threshold field of the domain wall elementary motion for the explanation of polarization reversal anisotropy. Our main result is that the threshold field, as isotropic parameter, should be replaced by an anisotropic function of the wall orientation that is self-consistently defined by the polar properties and lattice pinning anisotropy of the ferroelectric. The proposed method for calculation of the anisotropic threshold field is not material-specific, thus the field should be anisotropic in all ferroelectrics with the spontaneous polarization anisotropy along the main crystallographic directions. The most evident examples are uniaxial ferroelectrics, layered ferroelectric perovskites and low symmetry incommensurate ferroelectrics.

The manuscript is organized in the following way. The introductive section I preceded the theoretical section II, which contains the problem statement for self-consistent numerical modeling and atomistic models explaining the origin of threshold field anisotropy. Results of numerical modeling of polarization dynamics is presented in the section III. Section IV demonstrates applicability of the proposed approach for quantitative interpretation of the experimental results [38]. Section V is a brief summary.

II. Theoretical description

2.1. Problem statement for self-consistent numerical modeling

Schematic of the tip-induced nanodomain formation on the non-polar Y-cut of uniaxial ferroelectric is shown in **Figure 2;** it is the same as in experiment [35]. The radial component of the axially-symmetric tip-induced electric field enables domain nucleation and growth. Since the radial component E_z is anti-symmetric, its maximum is located at some distance from the tip axes leading to the nanodomain displacement, as schematically shown in the figure.

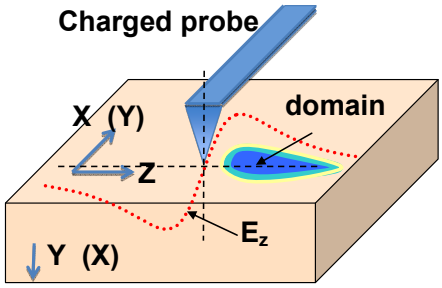

Figure 2. Schematics of the tip-induced polarization switching on the non-polar Y-cut of a uniaxial ferroelectric.

Electric potential φ satisfies electrostatic equations inside the layered system. Electric potential satisfies Laplace equation in the air/vacuum ambient semispace $-\infty < y < 0$. The potential is equal to the switching *dc* voltage at the surface of the tip. Inside a ferroelectric layer $0 < y < L$ the potential satisfies an anisotropic Poisson equation:

$$\varepsilon_{33}^{b}\frac{\partial^2\varphi_f}{\partial z^2}+\varepsilon_{11}\left(\frac{\partial^2\varphi_f}{\partial x^2}+\frac{\partial^2\varphi_f}{\partial y^2}\right)=\frac{1}{\varepsilon_0}\left(\frac{\partial P_z}{\partial z}-\rho\right), \quad (1)$$

Here ε_{33}^{b} is the background dielectric permittivity of the ferroelectric [45], ε_{11} is the transverse component of relative dielectric permittivity, ε_0 is a universal dielectric constant. Polarization gradient $\partial P_z/\partial z$ in the right-hand side of Eq.(1) reflects the existence of the bound charges originated from the inhomogeneous polarization distribution. Free charge density responsible for the bound charge

screening is ρ. Hereinafter we consider a proper wide-gap ferroelectric-semiconductor, such as $LiNbO_3$ without impurities, for which the charge density is $\rho(\varphi) = e\left(p(\varphi) - n(\varphi)\right)$, where equilibrium concentration free holes and electrons have a conventional form (see [46] and Appendix A in [47]).

Equation (1) should be supplemented with the boundary conditions of zero potential at bottom planar electrode, continuous potential and normal displacement at the interface between air and ferroelectric.

The ferroelectric polarization dynamics obeys relaxation-type differential equation with cubic nonlinearity (see Appendix A in [48]):

$$\tau_0 \frac{\partial \widetilde{P}_z}{\partial t} - \widetilde{P}_z + \widetilde{P}_z^3 - R_c^2\left(\frac{\partial^2 \widetilde{P}_z}{\partial z^2} + \frac{\partial^2 \widetilde{P}_z}{\partial y^2} + \frac{\partial^2 \widetilde{P}_z}{\partial x^2}\right) = \widetilde{E}_z \qquad (2)$$

Dimensionless polarization $\widetilde{P}_z = P_z / P_S$ is normalized on the spontaneous value $P_S = \sqrt{-\alpha/\beta}$. A soft phonon characteristic time $\tau_0 = -\Gamma/\alpha$ is determined by the ratio of kinetic Khalatnikov coefficient Γ and generalized dielectric stiffness $\alpha = \alpha_T\left(T - T_C\right)$, where T is temperature in Kelvins and T_C is Curie temperature. Correlation length $R_c = \sqrt{-g/\alpha}$ is about 1 nm far from T_C; g is the positive gradient coefficient. The electric field $E_z = -\partial\varphi/\partial z$ is normalized on the "threshold" field E_{th}, $\widetilde{E}_z = E_z / E_{th}$.

Despite the same mathematical form, in physical sense Equation (2) principally differs from the classical LGDK equation used previously [31-35, 37], because the threshold field E_{th} is not isotropic and equal to the thermodynamic coercive field, $E_c = 2\sqrt{-\alpha^3/27\beta}$. It is determined by the lattice pinning anisotropy that is dependent on the domain wall type and orientation with respect to the crystallographic axes. Consequently E_{th} can be anisotropic and much smaller than the thermodynamic coercive field.

The boundary conditions to Eq.(2) correspond to the uniform polarization far from the tip field action, $\widetilde{P}_z\left(r \to \infty\right) = +1$, and natural boundary conditions at the ferroelectric surfaces, $\partial\widetilde{P}_z/\partial y\big|_{y=0} = 0$ and $\partial\widetilde{P}_z/\partial y\big|_{y=L} = 0$.

2.2. Atomistic model explaining the threshold field anisotropy

The main original idea of our research is to demonstrate that threshold fields along different crystallographic directions can be significantly different due to crystal anisotropy of the inter-atomic relief and energy barriers. 3D-atomic structure of $LiNbO_3$ crystallographic cuts are shown in **Figure 3a-c** using the coordinates from Boysen and Altorfer [[48]]**.** A suggested step-like path of the domain wall motion in the polar direction Z on the non-polar X- and Y-cuts is shown by an elementary step in **Figures 3b-3c.** The step-like path, defined as the elementary Li-Li distances in the directions

perpendicular to the polar Z-axes, is in the agreement with Alikin et al explanation of the experimentally observed domain growth (see figure 4 in [38]). Then using rhombohedral lattice parameters of $LiNbO_3$, $a = 5.15$ Å, $c = 13.86$ Å, angle $\alpha_c = 55^o53'$ [49, 50], Z-, Y- and X-cuts schematics we calculated the minimal distances $p_{[abc]}$ between the equilibrium positions of uncharged domain wall planes at different crystallographic cuts, $p_{[100]} = \sqrt{3}a/2 \approx 4.460$ Å for X-cut, $p_{[010]} = a/2 \approx 2.575$ Å for Y-cut and $p_{[001]} = c/6 \approx 2.310$ Å for Z-cut.

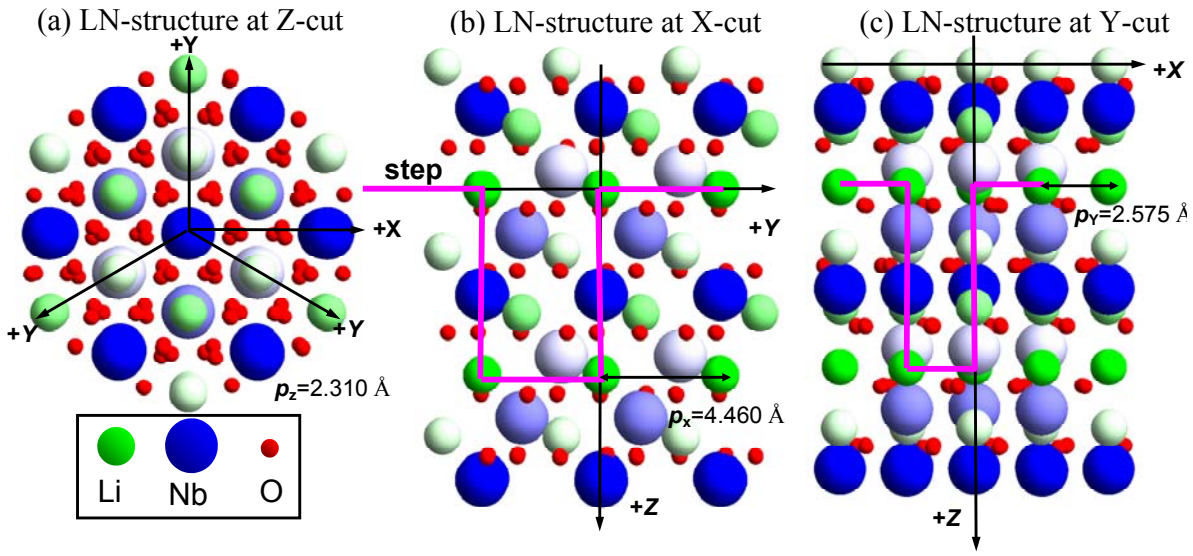

Figure 3. Atomic structure of $LiNbO_3$ Z-cut (XY plane) **(a)** X-cut (ZY plane) **(b)** and Y-cut (ZX-plane) **(c)**. Big blue balls are Nb atoms, smaller green balls are Li atoms and the smallest red balls are O atoms.

To calculate the anisotropic threshold field we account for the anisotropy of the minimal distance between the equilibrium positions of the uncharged domain wall in the S-I formula [40] in the following way

$$E_{th}^{[abc]} = -e^4 (\pi/2)^{7/2} \alpha P_S \left(w/p_{[abc]}\right)^3 \exp\left(-\pi^2 w/p_{[abc]}\right), \qquad (3)$$

Here the half-width of the domain wall w is normalized on the minimal distance $p_{[abc]}$ between the equilibrium positions of the uncharged domain wall plane propagating in the crystallographic direction [abc]. Hereinafter we associate [001] with a Z-cut, [010] with Y-cut and [001] with X-cut.

The anisotropic threshold field was calculated using Eq.(3) for $LiNbO_3$ parameters α, P_S and different domain wall half-width w, since the latter can be strongly affected by depolarization field and depends on the wall bound charge (e.g. incline angle with respect to the polar direction). Results are shown in the **Figure 4a**. As one can see, the value of E_{th} differs on the one or even several orders of magnitude for different direction of the domain wall motion. In addition it strongly decreases with

$p_{[abc]}$ increase and vary in the range (10^{-3} – 10^{+2}) kV/mm. E_{th} monotonically and rapidly decreases with w increase more than 1 Å for any period $p_{[abc]}$. Note, that smaller w values are unlikely physical. At fixed w> 1 Å the highest fields correspond to the smallest period $p_{[abc]}$, i.e. $E_{th}^{Z} < E_{th}^{Y} < E_{th}^{X}$ since $p_Z < p_Y < p_X$. This exactly means that the threshold field is the smallest for Z-cut, intermediate for Y-cut and the highest for the X-cut of the crystal.

To calculate the anisotropic activation field, that determines the nucleation process kinetics, we account for the anisotropy of the minimal distance between the equilibrium positions of the uncharged domain wall in the B-C approach [34] in the following way:

$$E_a^{[abc]} = \frac{1}{V_0}\frac{\gamma R}{UP_S}\sqrt{\ln\left(\frac{\gamma R\sqrt{\sigma_{\min}\delta\sigma}}{2p_{[abc]}P_S U}\right)\frac{\left(\sqrt{\sigma_{\min}\delta\sigma}\,p_{[abc]}\right)^3}{4\pi\varepsilon_0\varepsilon_{11}}}. \qquad (4)$$

Here V_0 is the elementary volume, U is the voltage applied to the tip, R is the effective tip size, γ is the dielectric anisotropy factor; $\sigma_{\min}$ is the minimal value of the periodic lattice potential and $\delta\sigma$ is the modulation depth of the domain wall energy $\sigma_W(x) \approx \sigma_{\min} + \delta\sigma\sin^2\left(\pi\left(x - x_0\right)/p_{[abc]}\right)$. The critical activation voltage of domain nucleation, U_{cr}, can be defined from the requirement of $\ln\left(\frac{\gamma R\sqrt{\sigma_{\min}\delta\sigma}}{2p_{[abc]}P_S U}\right) \geq 0$ in Eq.(4) that gives $U_{cr} = \frac{\gamma R\sqrt{\sigma_{\min}\delta\sigma}}{2p_{[abc]}P_S}$.

Activation field was calculated by Eq.(4) for parameters R, $\sigma_{\min}$ and $\delta\sigma$ from Ref.[34]. The results are shown in **Figure 4b**. The value of R is chosen in a reasonable agreement with effective pint charge model of the probe [51, 52]. As one can see, E_a is noticeably anisotropic. The dependence of E_a on the voltage U has a threshold-type; the field rapidly decreases with U increase and becomes zero $U > U_{cr}$, indicating the voltage threshold for instant nucleation. The value of U_{cr} depends on $p_{[abc]}$ as following $U_{cr}^{X} < U_{cr}^{Y} << U_{cr}^{X}$, because $p_Z < p_Y < p_X$.

Expressions (3)-(4) allowed us to estimate the ratio of the threshold and activation fields in different directions for known distances $p_{[abc]}$ and the energy profile of periodic lattice potential. Results are shown in **Figure 4c** and **4d.** The ratio of the threshold fields E_{th}^{X}/E_{th}^{Y} changes from 1.5 to 5, the ratios E_{th}^{Y}/E_{th}^{Z} and E_{th}^{X}/E_{th}^{Z} are within the range of 1.5 to 100 for realistic values of the domain wall width. The ratio of the activation fields E_a^{X}/E_a^{Y} changes from 1.5 to 10, the ratios E_a^{Y}/E_a^{Z} and E_a^{X}/E_a^{Z} are within the range of 0 to 3.

Note, that DFT calculations of the E_{th} values for three crystallographic directions can be very helpful for both our model verification and comparison with experiment. To the best of our knowledge the calculations are absent to date. Results of Ref.[34] only gives us corresponding equilibrium

position of the uncharged domain wall (determined as the center between two anion planes) and the values of the Y-wall energy relief, $\sigma_{min} = 0.160$ J/m^2 and $\delta\sigma = 0.150$ J/m^2 (see scheme in **Figure S1b**). The DFT parameters allowed estimating the activation field from Eq.(4) at applied voltage increase, but not E_{th}. Corresponding activation field E_a becomes essentially smaller than the thermodynamic coercive field E_c that is about 1.6 MV/cm for $LiNbO_3$ at room temperature(see **Figure 4b**).

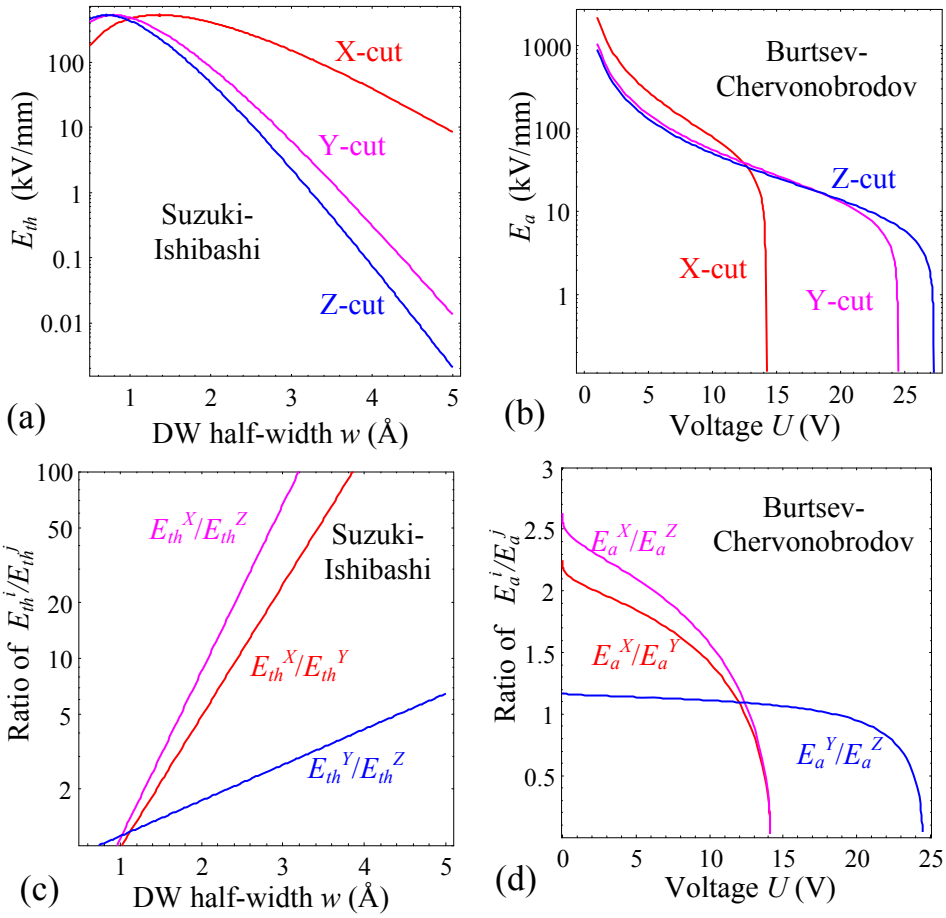

Figure 4. **(a)** Threshold fields dependence on the domain wall half-width w calculated within Suzuki-Ishibashi model for $LiNbO_3$ parameters $\alpha = -1.95\times10^9$ m/F, $P_S = 0.735$ C/m^2. **(b)** Activation fields dependence on the voltage U applied to the probe calculated within Burtsev-Chervonobrodov model for the parameters R=100 nm, $\sigma_{min} = 0.160$ J/m^2 and $\delta\sigma = 0.150$ J/m^2 [34]. **(c)** The threshold fields' ratio vs. the domain wall half-width w. **(d)** Activation fields' ratio vs. applied voltage U.

III. Modeling and interpolation of polarization dynamics

We solved numerically LGDK equation (2) for polarization together with the electrostatic equation (1) for different values of the free carriers concentration ρ. The concentration ρ was modeled the BPN

approximation, $\rho = n_0 \sinh(e\varphi/k_B T)$, for different values of equilibrium concentration n_0=0, 10^{14} cm^{-3}, 10^{16} cm^{-3}, 10^{18} cm^{-3}, 10^{19} cm^{-3}, and 10^{20} cm^{-3}. Appeared that calculated distributions of polarization and electric field were almost the same for $n_0 \leq 10^{19}$ cm^{-3}, because the screening length was still much higher than the effective probe size (~ 10 nm) and uncharged domain wall width (~ 1 nm). Thus we concluded that obtained numerical results are almost insensitive to the carrier concentration $\rho < 10^{19}$ cm^{-3}.

Our simulations showed that the concentrations n_0 higher than 10^{20} cm^{-3} can lead to the noticeable decrease of the probe electric field accompanied by the screening of the charged domain walls by free carries. These two factors result into essential decrease of the domain depth due to the screening as well as to the strong increase of the activation voltage required for the domain nucleation (up to an order of magnitude). Note, that the free carriers mostly affect on the domain sizes and domain wall conductivity in the doped ferroelectric-semiconductors, like $LiNbO_3$:Mg, where the free carriers concentration becomes more than 10^{20} cm^{-3} [53].

In contrast, the nanodomain shape and sizes evolution is relatively weakly affected by the bulk screening for the carrier concentration less than 10^{-19} cm^{-3}, which already seems too high value for wide-gap ferroelectric-semiconductor without impurities. Thus for the studied congruent $LiNbO_3$ without impurities one can neglect free carriers impact when model realistic experiments. On the other hand, the threshold field E_{th}, required for the domain wall motion along different crystallographic directions, is independent on the presence of free carriers, since it is defined from the minimal distance between the equilibrium atomic positions of domain wall.

To describe the congruent $LiNbO_3$ ferroelectric and dielectric properties at room temperature we used the following material parameters $\varepsilon_{33}{}^b = 5$, $\varepsilon_{11} = 84$, $\varepsilon_{33} = 30$, $\alpha = -1.95\times10^9$ m/F, g~10^{-10} V·m^3/C and $n_0 = 10^{18}$ cm^{-3}. Spontaneous polarization P_S =0.75 C/m^2 and correlation radius $R_c = \sqrt{-g/\alpha} \approx$(0.4 – 1) nm. Threshold field vary in the range E_{th} = (21 – 550) kV/mm. The evolution of domain shape and corresponding depolarization field were calculated in COMSOL Multiphysics computational package.

Typical simulation results are shown in **Figure 5.** Colored domain cross-sections with solid borders are calculated in a self-consistent way for different threshold fields, E_{th} = 50 kV/mm for Y-cut and E_{th} = 550 kV/mm for X-cut correspondingly. Dotted ellipse-like curves imposed on the colored domains are the domain cross-sections calculated under the assumptions that the depolarization field is the same as created by the semi-ellipsoid with infinitely thin domain wall; and the threshold field is the same for X- and Y-cuts. So that the figure illustrates strong differences between the domains cross-

sections calculated within not self-consistent (dotted curves) and self-consistent approaches (solid curves) side-by-side.

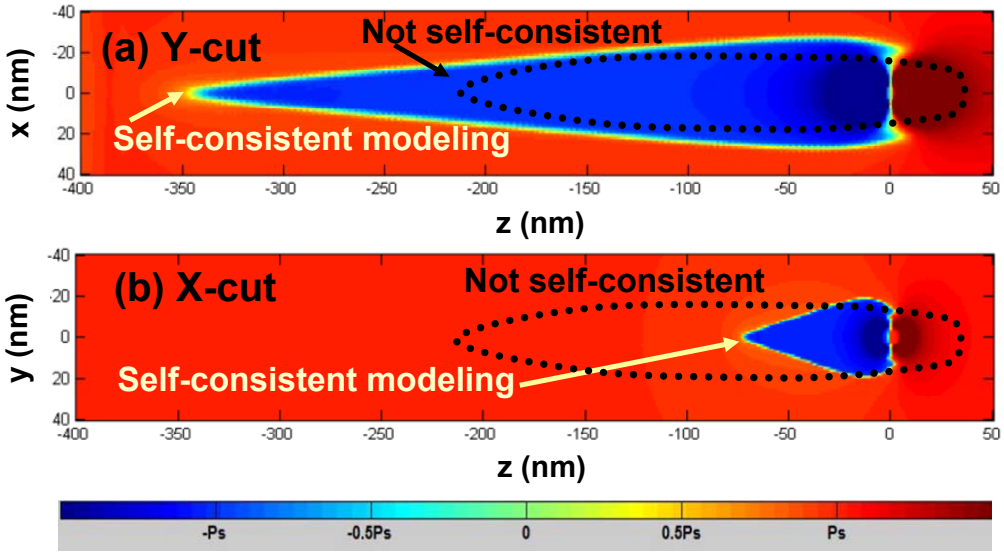

Figure 5. Domain shape (top view) calculated for Y-cut **(a)** and X-cut **(b)**. Colored domain cross-sections with solid borders are calculated in a self-consistent way for different threshold fields E_{th} = 50 kV/mm for Y-cut and E_{th} = 550 kV/mm for X-cut. Domain cross-sections shown by dotted ellipse-like curves are calculated under the assumptions that the threshold field is the same for X- and Y-cuts, depolarization field is the same as created by the semi-ellipsoidal domains, domain walls are infinitely thin.

The domain shape on the Y-cut (as well as on the X-cut) calculated self-consistently is close to the cone prolonged in the polar direction Z, at that the length rapidly increases with the threshold field decrease. The shape strongly deviates from the semi-ellipsoidal one, in contrast to the suggestions made earlier in order to obtain analytical expressions for the depolarization electric field energy [39]. The domain wall thickness increases in the immediate vicinity of the charged domain apex in order to decrease the strong depolarization field. As one can conclude from the figure only self-consistent approach lead to the quantitative agreement between the calculated domain shape and sizes and experimental results shown in **Figures 1b,c**.

Thus the absence of self-consistency in the calculations of the electric fields (not only the threshold field E_{th}, but also the field $\widetilde{E}_z = E_z/E_{th}$, that stands in the right-hand side of Eq.(2) for polarization P_z) leads to the incorrect domain's shape and sizes (primary length). Actually the field $E_z = -\partial\varphi/\partial z$ should be determined in agreement with the Poisson Eq.(1) for the potential φ_f that in turn include the polarization derivative $\partial P_z/\partial z$ in the right-hand side. Thus Eq.(1) and (2) are strongly

coupled and should be solved together in a self-consistent manner. If we ignore the threshold field anisotropy and the coupling between the electric field and polarization in the Poisson equation, for instance by assuming some concrete form of the depolarization field, e.g. using the field caused by semi-ellipsoidal domain, as it was done Pertsev et al [39], the charged probe induces the semi-ellipsoidal domain with equal length and width at both non-polar cuts X and Y. The result is in a strong disagreement with experiment of Alikin et al [38], as well as with the results of self-consistent calculations.

In order to perform comparative analysis of the domain evolution, we extracted the temporal dependencies of the sizes from the simulated domain profiles. Using designations from the **Figure 1a** we calculated the temporal evolution of the domain length $l(t)$ (**Fig. 6a**), width $r(t)$ (**Fig. 6b**) and apex angle $\theta(t)$ (**Fig. 7a**).

Figures 6a and **6b** illustrate the dependencies of the domain length and maximal width on the ferroelectric surface versus the pulse duration. Points correspond to the numerical results simulated in COMSOL. The dependencies are calculated for different values of the threshold field E_{th}. The domain sizes monotonically decreases with E_{th} increasing. During the activation stage corresponding to the times from 0 to 0.5 t/τ_0 the domain length increases super-linearly, the width increases sub-linearly. Starting from the times $t>0.5\tau_0$ all the sizes asymptotically obey the logarithmic law, $l(t) \sim \log(t/t_c)$.

Following the available experiments [8, 9] and nucleation rate theory [27, 54, 55] domain sizes $s(t)$ obey the logarithmic law versus the writing time, e.g. $s(t) \sim \log(t/t_c)$. Allowing for the existence of the activation voltage in accordance with B-C model, domain sizes should change rapidly at small writing times, since the domain wall velocity exponentially depends on the dragging electric field [9, 13]. These facts motivate us to interpolate the numerical data by the function $s(t) \sim C^S f(t/t_0)\log(t/t_c - 1) + B^S$ with the fitting parameters C^S, t_0, t_c and B^S. Hence, to establish an analytical dependence of the domain sizes vs. writing time we performed the fitting of the simulated results by the following interpolation functions:

$$l(t) = \frac{C_k^l (t/t_{0k})^{3/2}}{(t/t_{0k})^{3/2} + 1} \log\left((t/t_{ck}) - 1\right) + B_k^l, \tag{5}$$

$$r(t) = C_k^r \log\left((t/t_{ck}) - 1\right) + B_k^r. \tag{6}$$

The subscript $k=1-5$ corresponds to the value of the threshold field E_{th} = (21, 50, 100, 200, 550) kV/mm. The interpolation functions for the domain sizes have sense for writing times $t > t_{ck}$, indicating the impossibility to write a stable domain by a shorter pulse. Also $f(t >> t_c) \to 1$.

Figures 6c and **6d** show the dependencies of the constants B_k, C_k and t_{ck} on the threshold field E_{th}. The value $B_k^{l,r}$ monotonically decreases and t_{ck} monotonically increases with E_{th} increasing. As anticipated, the critical times t_{c1}=0.065, t_{c2}=0.06, t_{c3}=0.05, t_{c4}=0.03 and t_{c5}=0.02 are the same for the domain length and width. The value C_k^l monotonically decreases, while C_k^r very slightly increases with E_{th} increasing.

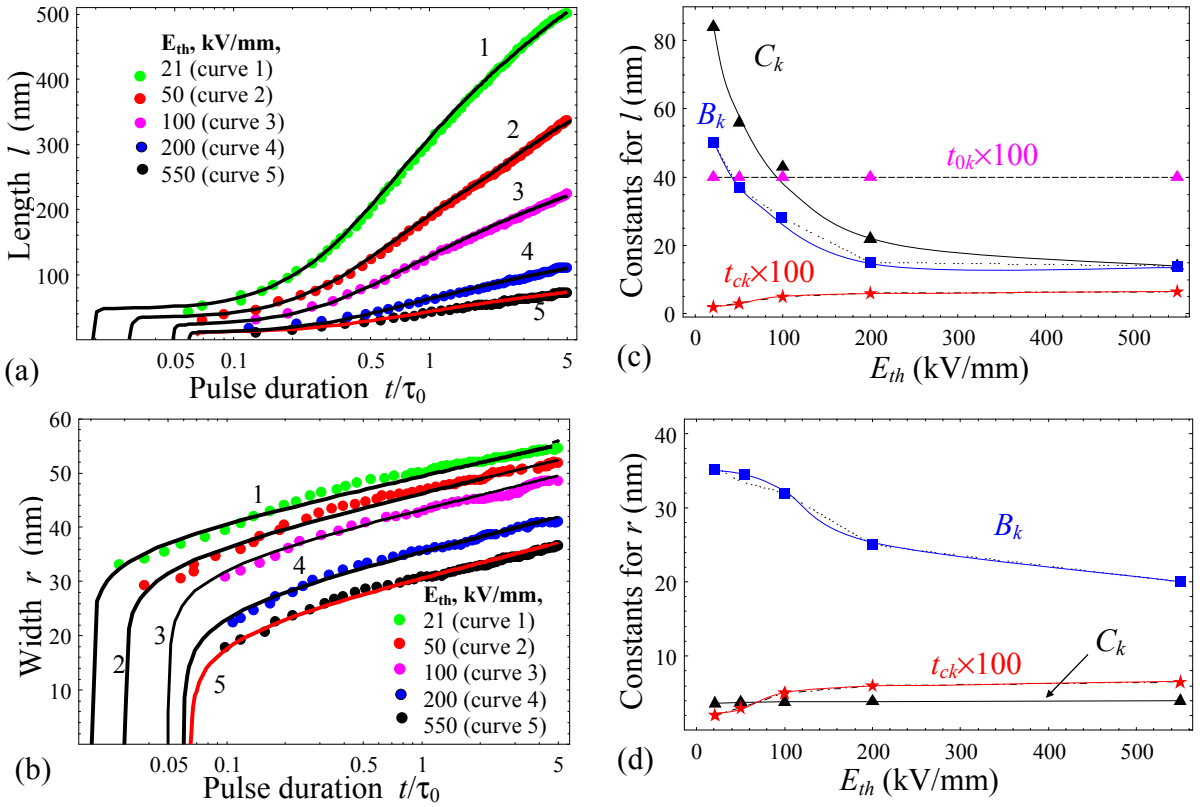

Figure 6. Temporal dependencies of the domain length **(a)** and width **(b)** on the ferroelectric surface calculated for different threshold fields E_{th} = (21, 50, 100, 200, 550) kV/mm. Points correspond to the numerical results simulated in COMSOL. Solid curves 1-5 correspond to the interpolation functions: **(a)** Eq.(5) plotted for parameters C_k, B_k, t_{0k} and t_{ck} shown in the plot (c). **(b)** Eq.(6) plotted for parameters C_k, B_k and t_{ck} shown in the plot d. The scale for t_{ck} and t_{0k} are 10^2. **(c,d)** Dependence of the fitting constants C_k, B_k and t_{ck} on the threshold field. As anticipated, the critical times t_{c1}=0.065, t_{c2}=0.06, t_{c3}=0.05, t_{c4}=0.03 and t_{c5}=0.02 are the same for the plots **(a)-(b)**.

Temporal dependence of the angle θ is presented in **Figure 7a**. Points corresponding to the numerical results simulated in COMSOL are very different from the asymptotic expression $\theta_f = \arctan\sqrt{\varepsilon_{zz}/\varepsilon_{xx}}$ derived by Sidorkin [56] that gives the angle of the instability on the flat domain

about 19.65 deg for $LiNbO_3$. Note that this expression does not account for the increase of the domain wall thickness near charged apex and thus it appears essentially overestimated with respect to values calculated numerically. Hence, to establish the analytical law of the angle dependence on time, we performed the fitting of the simulated results by the following interpolation function:

$$\theta(t) = C_k^\theta + B_k^\theta \exp(-t/t_{0k}). \quad (7)$$

The constant C_k^θ doesn't have to coincide with the value of θ_f. Similarly to width and length fitting, the subscript k=1 – 5 corresponds to different E_{th} values. As one can see from **Figure7a,** the angle is acute, monotonically decreases and saturates in agreement to Eq.(7). As it follows from **Figure 7b** the constant B_k monotonically increases with the E_{th} and saturates for E_{th} >200 kV/mm. The constant C_k monotonically increases with E_{th} increasing; the saturation is possible for E_{th} >500 kV/mm, which is beyond the simulation range.

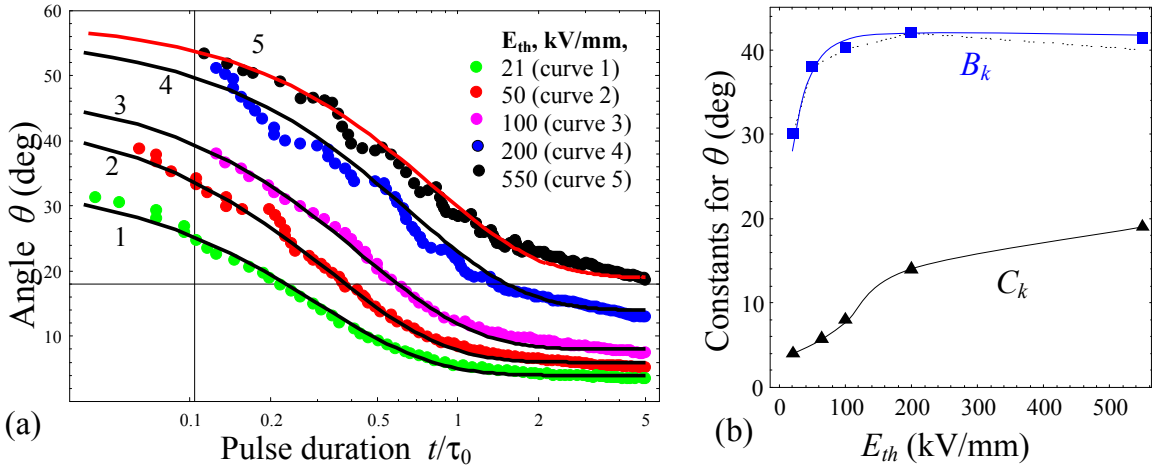

Figure 7. (a) Temporal dependence of the domain apex angle θ calculated for different threshold fields E_{th} = (21, 50, 100, 200, 550) kV/mm. Points correspond to the numerical results simulated in COMSOL. Solid curves 1-5 are the interpolation functions (7) plotted for parameters C_1=4; C_2=6; C_3=8; C_4=14; C_5=19; B_1=30; B_2=38; B_3=40; B_4=42; B_5=42; t_{01}=0.3; t_{02}=0.33; t_{03}=0.43; t_{04}=0.60; t_{05}=0.8. **(b)** Dependence of the constants C_k and B_k on the threshold field.

IV. Comparison of domain shape and sizes with experiment

Alikin et al [38] measured experimentally the domain shape and sizes on the non-polar X- and Y-cuts of CLN. Corresponding domain length and width at the non-polar surfaces of the CLN are shown by symbols with error bars in **Figures 8a** and **8b**. Solid curves are interpolated functions for the domain sizes given by Eq.(5) and (6) with the best fitting parameters listed in the capture. Using the parameters for domain length we calculated the ratios $B_Y/C_Y = 0.73$ for Y-cut and $B_X/C_X = 0.89$ for

X-cut. This can be compared with values extracted from COMSOL modeling as it shown in **Figure 8c-d**. After placing the points B_Y/C_Y and B_X/C_X in **Figure 8c-d** we concluded that the threshold field E_{th} for X-cut is about 420 kV/mm and about 250 kV/mm for Y-cut. Note that the best fitting parameters for domain width corresponding to the same values of E_{th}^X and E_{th}^Y is C_Y=23, B_Y=138, C_X=15, B_X=82.5.

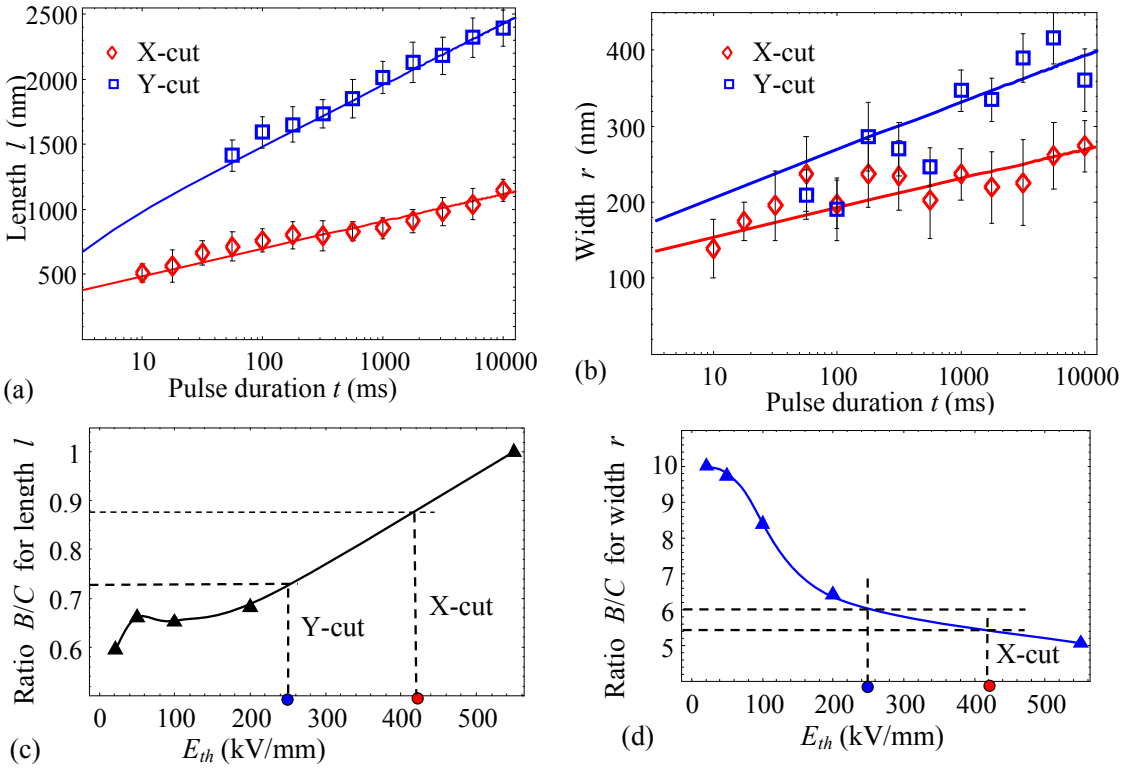

Figure 8. Dependencies of **(a)** domain length and **(b)** domain width vs. the switching pulse duration on X- and Y-cuts of $LiNbO_3$. Symbols with error bars are experimental data [38] for X- and Y- cuts of 20-μm-thick CLN placed in dry nitrogen, solid curves are our fitting using the interpolation functions (5)-(6). The function for the domain length is Eq.(5) with parameters C_X=90, B_X=80, t_{cX}=0.1 ms, t_{0X}=1 ms for X-cut and C_Y=205, B_Y=150, t_{cY}=0.15 ms, t_{0Y}=1 ms for Y-cut. The function for the domain width is Eq.(6) with parameters C_Y=23, B_Y= 138, t_{cY}=0.15 ms for Y-cut, C_X= 15, B_X=82.5 and t_{cX}=0.1 ms for X-cut. **(c-d)** The ratio B/C extracted from numerical modeling.

Note that due to the scattering of the width for X- and especially Y-cut the experimental data for domain width is much less reliable than the data for length. So that it has a little sense to conclude about the method validity from the domain width fitting. However we obtained a reasonable agreement with experiment by changing the fitting parameters for both domain length and width.

Finally, let us discuss the question about the difference in domain depth for the cases when the writing electric field acts on different $LiNbO_3$ cuts. As it was reported earlier by Molotskii et al [9] for

the case of nanodomain formation on polar Z-cut their depth (called length in the ref.[9] because of the radial symmetry of domain cross-section) can reach micron distances due to the breakdown effect. Alikin et al [38] concluded from a selective etching that the domain depth on the Y-cut is rather small in comparison with the one on the X-cut. Moreover, "Y-cut domains" most likely remained nanosized in Y-direction, while "X-cut domain" can be much deeper, but not needle-like as "Z-cut domains".

Our approach can explain these facts, because it account for the anisotropy of lattice barriers and depolarization effects at the charged domain walls. In particular, the longest needle-like shape of Z-cut domains is conditioned by the smallest threshold field $E_{th}(p_Z)$ and domain breakdown in Z-direction takes place. The smallest depth Y-cut domain in X-direction originated from inequality $E_{th}(p_X) >> E_{th}(p_Y) > E_{th}(p_Z)$, since the smaller is the threshold field the bigger is the domain size. These speculations can be quantified using the $E_{th}(p_{[abc]})$ ratios for different crystallographic cuts presented in **Figure 4c** and corresponding minimal distance $p_Z \approx 2.310$ Å, $p_Y \approx 2.575$ Å, $p_X \approx 4.469$ Å**.**

V. Conclusion

We quantitatively explained the physical nature of anisotropic nanodomain formation induced by the biased SPM tip on polar and non-polar cuts of uniaxial ferroelectrics. Our self-consistent approach takes into account crystallographic anisotropy of lattice pinning barriers and so corresponding threshold field becomes dependent on the crystallographic direction. Performed analysis proved that the threshold field for X-cut should be significantly higher than the one for Y-cut and Z-cut. Corresponding analytical expression for the anisotropic threshold field was obtained within modified Suzuki-Ishibashi approach, which allows us to explain quantitatively several times difference in nanodomain length on the X- and Y-cuts observed experimentally in $LiNbO_3$ [38]..

Our main result is the conception of anisotropic threshold field of the domain wall elementary motion. The proposed method for calculation of the field is not ferroelectric material-specific. We predict that the threshold field should be anisotropic in all ferroelectrics with the spontaneous polarization anisotropy along the main crystallographic directions X, Y and Z. The most evident examples are all uniaxial ferroelectrics (e.g. $LiNbO_3$, $LiTaO_3$, KDP, TGS, Rochelle salt, PVDF), layered ferroelectrics (e.g. SBT, SBTN, $Bi_4Ti_3O_{12}$), incommensurate ferroelectrics like $Sn_2P_2(S,Se)_6$ and $CuInP_2(S,Se)_6$ as well as their solid solutions with other ferroics. The field can be isotropic only in the multiaxial ferroelectric with cubic parent phase (e.g. in perovskites $BaTiO_3$, $PbTiO_3$, $KNbO_3$ and likely in $BiFeO_3$). To the best of our knowledge all previous analytical models regarded the field isotropic for all ferroelectrics. Hence obtained results can give insight into nontrivial anisotropic dynamics of polarization reversal at the nanoscale.

Acknowledgements

E.A.E. and A.N.M. acknowledge National Academy of Sciences of Ukraine (grants 35-02-15). V.Ya.S. acknowledges RFBR (grant 14-02-90447 Ukr-a). A portion of this research (A.V.I, S.V.K.) was conducted at the Center for Nanophase Materials Sciences (project CNMS2016-061), which is a DOE Office of Science User Facility.

Authors contribution. A.N.M. formulated and elaborated the theoretical model, derived corresponding analytical expressions and wrote the initial text of the manuscript with illustrations. A.I. performed corresponding numerical simulations of domain shape and sizes in COMSOL, the numerical results processing and smoothing jointly with O.V.V. Y.M.F. performed the fitting of the COMSOL results by interpolation functions. E.A.E. densely worked on the improvement of the anisotropic threshold field model and correlation with experiment of the obtained theoretical results. A.N.M., A.V.I., V.V.O, V.Ya.S., S.V.K. and E.A.E. tightly worked on the physical interpretation of the obtained theoretical results, improvement of the paper text, discussion and conclusions.

References

[1.] J.F. Scott. "Nanoferroelectrics: statics and dynamics." J. Phys.: Condens. Matter 18, R361-R386 (2006).

[2] A Gruverman and A Kholkin "Nanoscale ferroelectrics: processing, characterization and future trends." *Rep. Prog. Phys*. **69** 2443 (2006).

[3] M. Alexe and A. Gruverman (eds), *Nanoscale Characterization of Ferroelectric Materials* (Heidelberg: Springer, 2004)

[4] S.V. Kalinin and A. Gruverman (eds), *Scanning Probe Microscopy of Electrical and Electromechanical Phenomena at the Nanoscale* (Berlin: Springer, 2007)

[5] S.V. Kalinin, A.N. Morozovska, Long Qing Chen, Brian J. Rodriguez "Local polarization dynamics in ferroelectric materials" Rep. Prog. Phys. 73, 056502-1-67 (2010).

[6] S.V. Kalinin, B.J. Rodriguez, S. Jesse, E. Karapetian, B. Mirman, E.A. Eliseev, A.N. Morozovska "Nanoscale Electromechanics of Ferroelectric and Biological Systems : A New Dimension in Scanning Probe Microscopy (review)" Annual Review of Materials Research 37, 189–238 (2007).

[7] A. V. Ievlev, S. V. Kalinin. "Data Encoding Based on the Shape of the Ferroelectric Domains Produced by Using a Scanning Probe Microscope Tip". Nanoscale 7(36), 11040 (2015).

[8] B.J. Rodriguez, R. J. Nemanich, A. Kingon, Alexei Gruverman, S. V. Kalinin, K. Terabe, X. Y. Liu, and K. Kitamura. "Domain growth kinetics in lithium niobate single crystals studied by piezoresponse force microscopy." Appl. Phys. Lett. 86, 012906 (2005).

[9] M. Molotskii, A. Agronin, P. Urenski, M. Shvebelman, G. Rosenman, Y. Rosenwaks. "Ferroelectric Domain Breakdown." Phys. Rev. Lett. .90, 107601 (2003).

10.J. Woo, S. Hong, N. Setter, H. Shin, J.-U. Jeon, Y.E. Pak, K. No "Quantitative analysis of the bit size dependence on the pulse width and pulse voltage in ferroelectric memory devices using atomic force microscopy" J. Vac. Sci. Technol. B. 19, 818-824 (2001).

[11.] M.I. Molotskii, M.M. Shvebelman "Dynamics of ferroelectric domain formation in an atomic force microscope." *Philosophical Magazine* 85, 1637-1655 (2005).

12. M. Abplanalp "Piezoresponse Scanning Force Microscopy of Ferroelectric Domains" A dissertation submitted to the Swiss Federal Institute of Technology for the degree of Doctor of Natural Sciences (Zurich, 2001). – 208 p.

13. A. Agronin, M. Molotskii, Y. Rosenwaks, G. Rosenman, B.J. Rodriguez, A.I. Kingon, and A. Gruverman "Dynamics of ferroelectric domain growth in the field of atomic force microscope." J. Appl. Phys. 99, 104102 (2006).

[14.] S. Hong, B. Ecabart, E.L. Colla, and N. Setter. "Three-dimensional ferroelectric domain imaging of bulk $Pb(Zr,Ti)O_3$ by atomic force microscopy" Appl. Phys. Lett. 84, 2382-2384 (2004).

[15.] Igor Stolichnov, Lisa Malin, Enrico Colla, Alexander K. Tagantsev, and Nava Setter. "Microscopic aspects of the region-by-region polarization reversal kinetics of polycrystalline ferroelectric Pb (Zr, Ti) O3 films." Appl. Phys. Lett. 86, 012902 (2005).

16. S.V. Kalinin, D.A. Bonnell "Local potential and polarization screening on ferroelectric surfaces" Phys. Rev. B 63, 125411 (2001).

[17] Ievlev, A. V., Jesse, S., Morozovska, A. N., Strelcov, E., Eliseev, E. A., Pershin, Y. V., Kumar, A., Shur, V. Y. & Kalinin, S. V. Intermittency, Quasiperiodicity and Chaos in Probe-Induced Ferroelectric Domain Switching. *Nature Physics* **10**, 59 (2014).

[18]. A.L. Kholkin, I. K. Bdikin, V. V. Shvartsman, and N. A. Pertsev. "Anomalous polarization inversion in ferroelectrics via scanning force microscopy." *Nanotechnology* 18, 095502 (2007).

19. S. Bühlmann, E. Colla, and P. Muralt. "Polarization reversal due to charge injection in ferroelectric films." *Physical Review B* 72, 214120 (2005).

[20]. Y. Kim, S. Bühlmann, S. Hong, S-H. Kim, K. No "Injection charge assisted polarization reversal in ferroelectric thin films" App. Phys. Lett. 90, 072910 (2007).

[21] A.V. Ievlev, Morozovska, A. N., Eliseev, E. A., Shur, V. Y. & Kalinin, S. V. Ionic Field Effect and Memristive Phenomena in Single-Point Ferroelectric Domain Switching. *Nature Communication* **5**, 5545 (2014).

[22]. V.Ya. Shur "Domain Nanotechnology in Lithium Niobate and Lithium Tantalate Crystals." Ferroelectrics, **399**, 97-106 (2010).

[23]. P.S. Zelenovskiy, V.Ya. Shur, P. Bourson, M.D. Fontana, D.K. Kuznetsov, and E.A. Mingaliev, "Raman Study of Neutral and Charged Domain Walls in Lithium Niobate" Ferroelectrics, **398**, 34-41. (2010).

[24] . V.Ya. Shur, D.K. Kuznetsov, E.A. Mingaliev, E.M. Yakunina, A.I. Lobov, and A.V. Ievlev."In situ Investigation of Formation of Self-assembled Nanodomain Structure in Lithium Niobate after Pulse Laser Irradiation" Appl. Phys. Lett., **99**, 082901 (2011).

[25] . V.Ya. Shur, M.S. Nebogatikov, D.O. Alikin, P.S. Zelenovskiy, M.F. Sarmanova, A.V. Ievlev, E.A. Mingaliev, and D.K. Kuznetsov. "Investigation of the Nanodomain Structure Formation by Piezoelectric Force Microscopy and Raman Confocal Microscopy in $LiNbO_3$ and $LiTaO_3$ Crystals" J. Appl. Phys., **110**, 052013 (2011).

[26.] R. Landauer "Electrostatic Considerations in $BaTiO_3$ Domain Formation during Polarization Reversal" J. Appl. Phys. 28, 227-234 (1957).

[27.] M. Molotskii "Generation of ferroelectric domains in atomic force microscope" J. Appl. Phys. **97**, 6234 (2005).

[28.] M. Shvebelman. "Static and dynamic properties of ferroelectric domains studied by atomic force microscopy" Thesis submitted for the degree of "Doctor of Philosophy" (Tel Aviv University, 2005). 315 p.

[29.] S.V. Kalinin, Alexei Gruverman, Brian J. Rodriguez, Junsoo Shin, Arthur P. Baddorf, E. Karapetian, and M. Kachanov. "Nanoelectromechanics of polarization switching in piezoresponse force microscopy." J. Appl. Phys. 97, 074305 (2005).

[30.] A.Yu. Emelyanov "Coherent ferroelectric switching by atomic force microscopy" Phys. Rev. B. Vol.71, 132102 (2005).

[31] A.N. Morozovska, S.V. Svechnikov, E.A. Eliseev, S. Jesse, B.J. Rodriguez, S.V. Kalinin "Piezoresponse Force Spectroscopy of Ferroelectric-Semiconductor Materials" J. Appl. Phys. 102, № 11, 114108-1-14 (2007).

[32] A.N. Morozovska, S.V. Kalinin, E.A. Eliseev, V. Gopalan, S.V. Svechnikov "The Interaction of an 180-degree Ferroelectric Domain Wall with a Biased Scanning Probe Microscopy Tip: Effective Wall Geometry and Thermodynamics in Ginzburg-Landau-Devonshire Theory" Phys. Rev. B. 78, № 12, 125407 (2008).

[33] A.N. Morozovska, E.A. Eliseev, Yulan Li, S.V. Svechnikov, P. Maksymovych, V.Y. Shur, Venkatraman Gopalan, Long-Qing Chen, and S.V. Kalinin "Thermodynamics of nanodomain formation and breakdown in Scanning Probe Microscopy: Landau-Ginzburg-Devonshire approach" Phys. Rev. B. 80, 214110 (2009).

[34] Vasudeva Rao Aravind, A.N. Morozovska, S. Bhattacharyya, D. Lee, S. Jesse, I. Grinberg, Y.L. Li, S. Choudhury, P. Wu, K. Seal, A.M. Rappe, S.V. Svechnikov, E.A. Eliseev, S.R. Phillpot, L.Q. Chen, Venkatraman Gopalan, S.V. Kalinin "Correlated polarization switching in the proximity of a 180° domain wall" Phys. Rev. B 82, 024111-1-11 (2010).

[35] Anton V. Ievlev, Denis O. Alikin, Anna N. Morozovska, Olexander V. Varenyk, Eugene A. Eliseev, Andrei L. Kholkin, Vladimir Ya Shur, and Sergei V. Kalinin. "Symmetry Breaking and Electrical Frustration during Tip-Induced Polarization Switching in the Nonpolar Cut of Lithium Niobate Single Crystals." *ACS nano* 9, 769-777 (2014).

[36] P. Maksymovych, S. Jesse, M. Huijben, R. Ramesh, A.N. Morozovska, S. Choudhury, L.-Q. Chen, A.P. Baddorf, S.V. Kalinin // Intrinsic nucleation mechanism and disorder effects in polarization switching on ferroelectric surfaces / Phys. Rev. Lett. 102, №1, 017601 (2009).

[37] A.N. Morozovska, E.A. Eliseev, Yulan Li, S.V. Svechnikov, P. Maksymovych, V.Y. Shur, Venkatraman Gopalan, Long-Qing Chen, and S.V. Kalinin // Thermodynamics of nanodomain formation and breakdown in Scanning Probe Microscopy : Landau-Ginzburg-Devonshire approach / Phys. Rev. B. 80, 214110 (2009).

[38] D. O. Alikin, A. V. Ievlev, A. P. Turygin, A. I. Lobov, S. V. Kalinin, and V. Ya. Shur, Tip-induced domain growth on the non-polar cuts of lithium niobate single-crystals. Appl. Phys. Lett. **106**, 182902 (2015)

[39] N. A. Pertsev and A. L. Kholkin, "Subsurface nanodomains with in-plane polarization in uniaxial ferroelectrics via scanning force microscopy." Phys. Rev. B **88**, 174109 (2013).

[40] S. Choudhury, Y. Li, N. Odagawa, Aravind Vasudevarao, L. Tian, P. Capek, V. Dierolf, A. N. Morozovska, E.A. Eliseev, S.V. Kalinin, Y. Cho, L.-Q. Chen, V. Gopalan "The influence of 180° ferroelectric domain wall width on the threshold field for wall motion" J. Appl. Phys. 104, № 8, 084107 (2008)

[41] Y. Ishibashi, "Computational Method of Activation Energy of Thick Domain Walls." J. Phys. Soc. Jpn. **46**, 1254 (1979).

[42] R. Miller and G. Weinreich, "Mechanism for the sidewise motion of 180 domain walls in barium titanate" Phys. Rev. **117**, 1460 (1960).

[43] E. V. Burtsev and S. P. Chervonobrodov, " Some problems of 180°-switching in ferroelectrics " Ferroelectrics **45**, 97 (1982).

[44] Y. H. Shin, I. Grinberg, I. W. Chen, and A. M. Rappe, "Nucleation and growth mechanism of ferroelectric domain-wall motion." Nature, London, **449**, 881 (2007).

[45] A. K. Tagantsev and G. Gerra. Interface-induced phenomena in polarization response of ferroelectric thin films. J. Appl. Phys. **100**, 051607 (2006).

[46] N.W. Ashcroft, N.D. Mermin, *Solid state physics* (Holt, Rinehart and Winston, New York, 1976) - 826 pages.

[47] Supplementary Materials [URL will be provided by Publisher]

[48] H. Boysen and F. Altorfer, "A neutron powder investigation of the high-temperature structure and phase transition in LiNbO3." *Acta Cryst. B* **50**, 405-414 (1994).

[49] S. C. Abrahams, J. M. Reddy, and J. L. Bernstein. "Ferroelectric lithium niobate. 3. Single crystal X-ray diffraction study at 24 C." Journal of Physics and Chemistry of Solids 27, no. 6: 997-1012 (1966).

[50] Yōichi Shiozaki, and Toshio Mitsui. "Powder neutron diffraction study of LiNbO 3." Journal of Physics and Chemistry of Solids 24, no. 8: 1057-1061 (1963).

[51] A.N. Morozovska, S.V. Svechnikov, E.A. Eliseev, S.V. Kalinin. "Extrinsic Size Effect in Piezoresponse Force Microscopy of Thin Films." Phys. Rev. B. 76, № 5, 054123-1-5 (2007).

[52] A.N. Morozovska, E.A. Eliseev, S.V. Kalinin. "The effective response and resolution function of surface layers and thin films in Piezoresponse Force Microscopy. J. Appl. Phys. 102, № 7, 074105 (2007).

[53] E.A. Eliseev, A.N. Morozovska, G.S. Svechnikov, Venkatraman Gopalan, and V. Ya. Shur, "Static conductivity of charged domain walls in uniaxial ferroelectric semiconductors" Phys. Rev. B 83, 235313 (2011).

[54] Jason Chen, Alexei Gruverman, Anna N. Morozovska and Nagarajan Valanoor. "Sub-Critical Field Domain Reversal in Epitaxial Ferroelectric Films." J. Appl. Phys. **116**, 124109 (2014)

[55] P. Paruch, T. Giamarchi, T. Tybell, and J. M. Triscone, "Nanoscale studies of domain wall motion in epitaxial ferroelectric thin films." J. Appl. Phys. **100**, 051608 (2006).

[56] A. S. Sidorkin Domain structure in ferroelectrics and related materials (Cambridge: Cambridge international science publishing 2006)